arXiv:1207.2251v1 [nucl-th] 10 Jul 2012

Analysis of ω self-energy at finite temperature and density in the real-time formalism

Sabyasachi Ghosh and Sourav Sarkar

July 11, 2012

Theoretical Physics Division, Variable Energy Cyclotron Centre,
1/AF, Bidhannagar, Kolkata 700064, India

Abstract

Using the real time formalism of field theory at finite temperature and density we have evaluated the in-medium ω self-energy from baryon and meson loops. We have analyzed in detail the discontinuities across the branch cuts of the self-energy function and obtained the imaginary part from the non-vanishing contributions in the cut regions. An extensive set of resonances have been considered in the baryon loops. Adding the meson loop contribution we obtain the full modified spectral function of ω in a thermal gas of mesons, baryons and anti-baryons in equilibrium for several values of temperature and baryon chemical potential.

1 Introduction

The in-medium properties of vector mesons has been a much discussed topic [1, 2]. One of the motivating factors is the possible connection with the partial restoration of the spontaneously broken chiral symmetry of QCD at high temperature and/or density. This is supplemented by the fact that the in-medium correlation function of vector currents of QCD, manifested in terms of the propagator of vector meson fields, can in fact be measured through the dilepton spectra unlike the axial current correlator where final state interactions corrupt the information [3]. Since the currents, with finite three-momentum can experience complex interactions with thermal excitations, the vector spectral function could exhibit new structures apart from the familiar shift of the peak and broadening of the width. The entire spectral shape is thus of interest.

A large volume of literature is dedicated to the study of vector mesons in the medium, the bulk of which concerns the ρ meson. Theoretical activities regarding the ω meson have been mostly performed in cold nuclear matter (see e.g. [4, 5] for a review). Though the lowest order virial expansion has been used in most cases [6, 7, 8] the approaches differ widely in their methods resulting in a large variation in the results concerning the mass and width. Consequently both positive and negative shifts of the peak position have been proposed. On the experimental front the situation is far from settled [4] with different groups reporting a reduction in mass [9] and increase in width [10] in pA and γA collisions respectively. The upcoming experiments at the FAIR facility at GSI thus assumes great significance in resolving some of the issues.

Finite temperature calculations at vanishing baryon density has been done in [11] showing a large increase in width due to $\omega \to 3\pi$ and $\omega\pi \to \pi\pi$ processes. Baryon induced effects on the ω spectral function at finite temperature has been treated within a virial approach in [12] where the self-energy is obtained in terms of empirical scattering amplitudes. In [13], in addition to contributions coming from scattering with mesons, resonance-hole contributions have been included in the self-energy.

Recently the ρ spectral function was evaluated at finite temperature and baryon density [14, 15] in which the sources modifying the free propagation of the ρ was obtained in a unified way from the branch cuts of the self-energy function. It was shown that the spectral strength at lower invariant masses was significantly enhanced due to contributions coming from the Landau cut which appears only in the medium and provides the effect of collisions of the ρ with the particles in the bath. Here we extend this analysis for the ω meson. For the baryonic contribution we have considered an extensive number of spin one-half and three-half resonances in the one-loop diagrams. These diagrams have been evaluated using the real time formulation of thermal field theory using the full relativistic baryon propagators in which baryons and anti-baryons appear on an equal footing. As a result, distant singularities coming from the unitary cut involving heavy baryons in the loop, which are neglected in certain approaches, are automatically included. They are found to contribute appreciably to the real part of the self-energy [16].

The article is organized as follows. In the following section we define the spectral function of the ω in terms of the diagonal component of the thermal self-energy matrix which appears in the real time formalism. In section 3 we evaluate the 11-component of the ω self-energy matrix for one-loop diagrams containing mesons and baryons and analyse their singularity structure. We have presented results of numerical evaluation of the real and imaginary parts of the self-energy as well as the spectral function of ω in section 4. We summarize and conclude in section 5. The details of the interaction Lagrangian and terms appearing in the self-energy have been provided in the appendix.

2 The full ω propagator in the medium

We begin with the complete ω-propagator in vacuum given by the Dyson equation,

$$D_{\mu\nu}(q) = D^{(0)}_{\mu\nu}(q) - D^{(0)}_{\mu\lambda}(q)\Pi^{\lambda\sigma}(q)D_{\sigma\nu}(q) \tag{1}$$

where

$$D^{(0)}_{\mu\nu}(q) = \left(-g_{\mu\nu} + \frac{q_\mu q_\nu}{m_\omega^2}\right)\Delta(q)\ ; \qquad \Delta(q) = \frac{-1}{q^2 - m_\omega^2 + i\epsilon} \tag{2}$$

is the free propagator.

In the real-time formulation of thermal field theory all two-point functions assume a 2×2 matrix structure on account of the contour in the complex time plane [17, 18]. As a result the Dyson equation for the full propagator in the medium is given by the matrix equation

$$D^{ab}_{\mu\nu}(q) = D^{(0)ab}_{\mu\nu}(q) - D^{(0)ac}_{\mu\lambda}(q)\Pi^{cd,\lambda\sigma}(q)D^{db}_{\sigma\nu}(q) \tag{3}$$

where a, b, c, d are thermal indices and take values 1 and 2. The free thermal propagator is given by

$$D^{(0)ab}_{\mu\nu}(q) = \left(-g_{\mu\nu} + \frac{q_\mu q_\nu}{m_\omega^2}\right)D^{ab}(q) \tag{4}$$

where the matrix D^{ab} has the components

$$\begin{aligned} D^{11} &= -(D^{22})^* = \Delta(q) + 2\pi i n\delta(q^2 - m_\omega^2) \\ D^{12} &= D^{21} = 2\pi i\sqrt{n(1+n)}\delta(q^2 - m_\omega^2) \end{aligned}$$

n being the Bose distribution function. The thermal indices can however be removed by diagonalization [19, 18] resulting in the equation

$$\overline{D}_{\mu\nu}(q) = \overline{D}^{(0)}_{\mu\nu}(q) - \overline{D}^{(0)}_{\mu\lambda}(q)\overline{\Pi}^{\lambda\sigma}(q)\overline{D}_{\sigma\nu}(q) \tag{5}$$

where the quantities with bars denote the corresponding diagonal components and in particular $\overline{D}^{(0)}_{\mu\nu}(q) = D^{(0)}_{\mu\nu}(q)$ as given in (2). Decomposing the self-energy function $\overline{\Pi}_{\mu\nu}(q)$ into transverse and longitudinal components using the projection operators $P_{\mu\nu}$ and $Q_{\mu\nu}$ respectively, eq. (5) can now be solved analogously as in vacuum to get

$$\overline{D}_{\mu\nu}(q) = \frac{-P_{\mu\nu}}{q^2 - m_\omega^2 - \overline{\Pi}_t(q)} + \frac{-Q_{\mu\nu}/q^2}{q^2 - m_\omega^2 - q^2\overline{\Pi}_l(q)} + \frac{q_\mu q_\nu}{q^2 m_\omega^2} \tag{6}$$

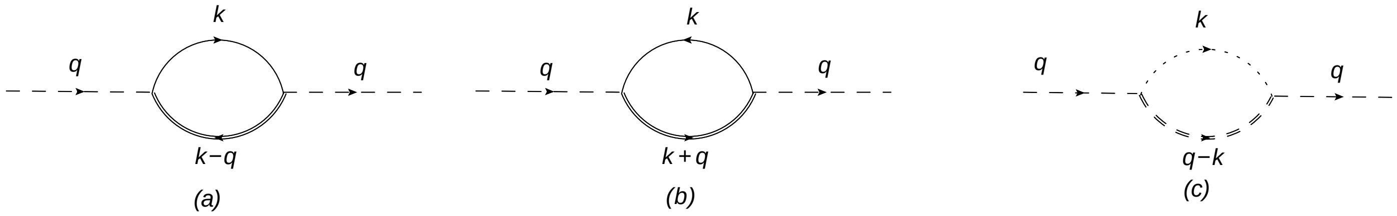

Figure 1: One-loop ω self-energy diagrams with baryons (a) & (b) where single and double lines represent nucleon (N) and resonances (B) respectively. Diagram (c) indicates meson loop where dashed, dotted and double dashed lines stand for ω, π and ρ respectively.

where [15]

$$P_{\mu\nu} = -g_{\mu\nu} + \frac{q_\mu q_\nu}{q^2} - \frac{q^2}{\overline{q}^2}\widetilde{u}_\mu\widetilde{u}_\nu,\ \widetilde{u}_\mu = u_\mu - (u\cdot q)q_\mu/q^2 \tag{7}$$

and

$$Q_{\mu\nu} = \frac{(q^2)^2}{\overline{q}^2}\widetilde{u}_\mu\widetilde{u}_\nu,\ \overline{q}^2 = (u\cdot q)^2 - q^2\ . \tag{8}$$

u_μ being the four-velocity of the thermal bath. The components of the self-energy function are defined as

$$\overline{\Pi}_t = -\frac{1}{2}(\overline{\Pi}^\mu_\mu + \frac{q^2}{\overline{q}^2}\overline{\Pi}_{00}), \qquad \overline{\Pi}_l = \frac{1}{\overline{q}^2}\overline{\Pi}_{00}, \quad \overline{\Pi}_{00} \equiv u^\mu u^\nu \overline{\Pi}_{\mu\nu} \tag{9}$$

which can be obtained from the 11-component of the in-medium self-energy matrix using

$$\begin{aligned} \mathrm{Re}\,\overline{\Pi}_{\mu\nu} &= \mathrm{Re}\,\Pi^{11}_{\mu\nu} \\ \mathrm{Im}\,\overline{\Pi}_{\mu\nu} &= \epsilon(q_0)\tanh(\beta q_0/2)\mathrm{Im}\,\Pi^{11}_{\mu\nu}\ . \end{aligned} \tag{10}$$

3 Analytical structure of ω meson self-energy

In this section we will evaluate one-loop diagrams of the type shown in Fig. 1 with mesons and baryons in the internal lines. The two cases are separately discussed below.

3.1 Baryon Loops

The internal lines in these loops contain a nucleon N and a baryon B which represents several spin one-half and three-half 4−star resonances. Here B stands for the $N^*(1440)$ $N^*(1520)$, $N^*(1535)$, $N^*(1650)$, $N^*(1720)$ resonances as well as the $N(940)$. For spin 1/2 resonances in the loop, the expression for 11-component of the ω self-energy in medium is given by

$$\Pi^{11,\mu\nu}(q) = iI_F \sum_{a=-1,+1}\int\frac{d^4k}{(2\pi)^4}Tr[\Gamma^\mu S^{11}(k,m_N)\Gamma^\nu S^{11}(k+aq,m_B)] \tag{11}$$

where S^{11} is the 11-component of the thermal propagator for fermions in the real-time formalism which is defined as $S^{11}(k,m) = (\not{k}+m)E^{11}(k,m)$ with

$$\begin{aligned} E^{11}(k,m) &= \frac{-1}{k^2-m^2+i\epsilon} - 2\pi i N(k_0)\delta(k^2-m^2); \qquad N(k_0) = n_+(\omega)\theta(k_0) + n_-(\omega)\theta(-k_0) \\ &= -\frac{1}{2\omega}\left(\frac{1-n_+}{k_0-\omega+i\epsilon} + \frac{n_+}{k_0-\omega-i\epsilon} - \frac{1-n_-}{k_0+\omega-i\epsilon} - \frac{n_-}{k_0+\omega+i\epsilon}\right) \end{aligned} \tag{12}$$

The function $n_\pm(\omega) = \dfrac{1}{e^{\beta(\omega \mp \mu_B)}+1}$ is the Fermi distribution for energy $\omega = \sqrt{\vec{k}^2+m^2}$ where the ± sign in the subscript refers to baryons and anti-baryons respectively and μ_B is the baryonic chemical potential which is taken to be equal for all baryons considered here. In the second line of eq. (12), the first and the second terms are associated with the propagation of baryons above the Fermi sea and holes in the Fermi sea respectively while the third and fourth terms represent the corresponding situation for anti-baryons [20]. The full relativistic baryon propagator thus treats the baryons and anti-baryons on an equal footing and the additional singularities which are not generally considered in usual approaches are automatically included. The two values of a in (11) correspond to the direct and crossed diagrams shown in Fig. 1 (a) and (b) respectively which are obtainable from one another by changing the sign of the external momentum q.

The corresponding expression for the case of loop graphs with spin 3/2 resonances is given by

$$\Pi^{11,\mu\nu}(q) = iI_F \sum_{a=-1,+1} \int \frac{d^4k}{(2\pi)^4} Tr[\Gamma^{\mu\alpha} S^{11}(k,m_N) \Gamma^{\nu\beta} S^{11}_{\beta\alpha}(k+aq,m_B)] \qquad (13)$$

where the spin-3/2 propagator, $S^{11}_{\mu\nu}(k,m) = (\not{k}+m)K_{\mu\nu}(k,m)E^{11}(k,m)$ with $K_{\mu\nu}(k,m) = -g_{\mu\nu} + \frac{2}{3m^2}k_\mu k_\nu + \frac{1}{3}\gamma_\mu\gamma_\nu + \frac{1}{3m}(\gamma_\mu k_\nu - \gamma_\nu k_\mu)$. Obtaining the vertex factors Γ^μ and $\Gamma^{\mu\alpha}$ from the interaction Lagrangians given in the appendix, both (11) and (13) can be expressed as

$$\Pi^{11,\mu\nu}(q) = iI_F \sum_{a=-1,+1} \int \frac{d^4k}{(2\pi)^4} L^{\mu\nu}(k,q) E^{11}(k,m_N) E^{11}(k+aq,m_B) \qquad (14)$$

where the isospin factor I_F is 2 for all the loops. The factor $L_{\mu\nu}(k,q)$ consists of a trace over Dirac matrices appearing in the two fermion propagators along with their associated tensor structure coming from the ωNB vertex.

Let us first discuss diagram (a) for which $a=-1$. The diagonal element of the in-medium self energy defined by eq. (10) after integration over k^0 can be written as

$$\begin{aligned} \overline{\Pi}^{\mu\nu}(q) &= \int \frac{d^3k}{(2\pi)^3} \frac{1}{4\omega_N\omega_B} \left[\frac{(1-n_+^N)L_1^{\mu\nu} - n_-^B L_3^{\mu\nu}}{q_0-\omega_N-\omega_B+i\eta\epsilon(q_0)} + \frac{n_+^N L_1^{\mu\nu} - n_+^B L_4^{\mu\nu}}{q_0-\omega_N+\omega_B+i\eta\epsilon(q_0)} \right. \\ &\quad \left. + \frac{-n_-^N L_2^{\mu\nu} + n_-^B L_3^{\mu\nu}}{q_0+\omega_N-\omega_B+i\eta\epsilon(q_0)} + \frac{n_-^N L_2^{\mu\nu} + (-1+n_+^B)L_4^{\mu\nu}}{q_0+\omega_N+\omega_B+i\eta\epsilon(q_0)} \right] \end{aligned} \qquad (15)$$

where $n^N \equiv n(\omega_N)$ with $\omega_N = \sqrt{\vec{k}^2+m_N^2}$, $n^B \equiv n(\omega_B)$ with $\omega_B = \sqrt{(\vec{k}-\vec{q})^2+m_B^2}$ and $L_i^{\mu\nu}, i=1,..4$ denote the values of $L^{\mu\nu}(k_0)$ for $k_0 = \omega_N, -\omega_N, q_0-\omega_B, q_0+\omega_B$ respectively. The imaginary part of (15) is trivially obtained and is given by

$$\begin{aligned} \mathrm{Im}\overline{\Pi}^{\mu\nu} &= -\epsilon(q_0)\pi \int \frac{d^3k}{(2\pi)^3} \frac{1}{4\omega_N\omega_B} [L_1^{\mu\nu}\{(1-n_+^N-n_-^B)\delta(q_0-\omega_N-\omega_B) \\ &\quad +(n_+^N-n_+^B)\delta(q_0-\omega_N+\omega_B)\} + L_2^{\mu\nu}\{(-n_-^N+n_-^B)\delta(q_0+\omega_N-\omega_B) \\ &\quad +(-1+n_-^N+n_+^B)\delta(q_0+\omega_N+\omega_B)\}] \end{aligned} \qquad (16)$$

in which the factors $L_{3,4}^{\mu\nu}$ have transformed into $L_1^{\mu\nu}$ or $L_2^{\mu\nu}$ on use of the associated δ-functions. The four δ-functions give rise to cuts in the self-energy function on the real axis in the complex energy plane and define the different kinematic domains where the imaginary part is non-zero. The first and fourth terms contribute for $q^2 > (m_B+m_N)^2$ and define the unitary cut and the second and third terms which are non-zero for $q^2 < (m_B-m_N)^2$ define the Landau cut. For a detailed discussion of the cuts in the complex q_0 plane see [14]. While the unitary cut is always present, the Landau cut appears only in the medium. In the case of the baryon loops only the Landau cut contribution is relevant to the imaginary part, the threshold for the unitary cuts being distant from the ω pole. It is easy to see that the imaginary part (coming from the Landau cuts) arises due to various scattering processes in which the ω is gained or lost during its propagation in the medium. For example, rearranging the statistical weights in the second term of eq. (16) as $(n_+^N - n_+^B) = n_+^N(1-n_+^B) - n_+^B(1-n_+^N)$, this term can be interpreted as the contribution to the imaginary part due to the disappearance of the ω by absorbing a nucleon from the heat bath to produce a higher mass baryon with the Pauli blocked probability $(1-n_+^B)$ minus the reverse process where it is produced along with the nucleon (which now suffers Pauli blocking) in the decay of the resonance B. The third term of eq. (16) can be analogously interpreted in terms of scattering with the anti-baryons.

The cut-structure for the second diagram (b) in Fig. 1 can also be analysed in the same way. Restricting to terms contributing to the physically relevant kinematic region $q^2,\ q_0 > 0$, the total contribution from the baryon loops is given by

$$\begin{aligned}\mathrm{Im}\,\overline{\Pi}^{\mu\nu}(q_0,\vec{q}) \;=\; & \frac{-\epsilon(q_0)}{16\pi|\vec{q}|}\int_{\widetilde{\omega}_N^+}^{\widetilde{\omega}_N^-} d\widetilde{\omega}_N[L_1^{\mu\nu}(a=+1)\{-n_+(\widetilde{\omega}_N)+n_+(\widetilde{\omega}_B=q_0+\widetilde{\omega}_N)\} \\ & + L_2^{\mu\nu}(a=-1)\{-n_-(\widetilde{\omega}_N)+n_-(\widetilde{\omega}_B=q_0+\widetilde{\omega}_N)\}]\end{aligned} \tag{17}$$

where $\widetilde{\omega}_N^{\pm} = \frac{S_N^2}{2q^2}(-q^0 \pm |\vec{q}|W_N)$ with $W_N = \sqrt{1-\frac{4q^2m_N^2}{S_N^4}}$, $S_N^2 = q^2 - m_B^2 + m_N^2$.

The real part of the self-energy can be obtained by evaluating the principal value integrals in eq. (15) which remain after the imaginary parts are removed. The terms within square brackets denoted by unity indicate the vacuum contribution to the real part of the self-energy. These divergent contributions from the baryonic loop as well as the mesonic loop discussed later are approximately taken into account by assuming that they renormalize the ω mass to its physical value. The terms with the Fermi distribution functions denote the medium contributions to the real part of the self-energy. These are finite owing to the natural cut-off provided by the thermal distribution functions. Note that at a given value of q the real part receives contribution from all the four terms unlike the imaginary part where the contribution depends on the associated δ-function.

The baryon resonances B have so far been considered in the narrow width approximation. For a realistic treatment it is necessary to include the width of the resonances. For this, we follow the procedure outlined e.g. in [21] of convoluting the self energy calculated in the narrow width approximation with the spectral function of the baryons as done for the ρ meson in [15]. This approach has the advantage that the analytic structure of the self energy discussed above is not disturbed.

$$\overline{\Pi}_B(q,m_B) = \frac{1}{N_B}\int_{m_B-2\Gamma_B}^{m_B+2\Gamma_B} dM \frac{1}{\pi}\mathrm{Im}\left[\frac{1}{M-m_B+\frac{i}{2}\Gamma_B(M)}\right]\overline{\Pi}_B(q,M) \tag{18}$$

with $N_B = \displaystyle\int_{m_B-2\Gamma_B}^{m_B+2\Gamma_B} dM \frac{1}{\pi}\mathrm{Im}\left[\frac{1}{M-m_B+\frac{i}{2}\Gamma_B(M)}\right]$ and $\Gamma_B(M) = \Gamma_{B\to N\pi}(M) + \Gamma_{B\to N\rho}(M)$; $M = \sqrt{q^2}$.

3.2 Meson loop

The 11-component of ω meson self energy for the $\rho\pi$ loop is given by

$$\Pi_{(\rho\pi)}^{11,\mu\nu}(q,m_\rho) = i\int\frac{d^4k}{(2\pi)^4}L^{\mu\nu}(k,q)D^{11}(k,m_\pi)D^{11}(q-k,m_\rho) \tag{19}$$

where D^{11} is the 11-component of the scalar propagator defined above. As before, the tensor structure associated with the two vertices and the vector propagator are included in $L^{\mu\nu}$, the details of which are given in the appendix. The diagonal element of the thermal self-energy matrix is obtained as

$$\begin{aligned}\overline{\Pi}_{(\rho\pi)}^{\mu\nu}(q,m_\rho) \;=\; & \int\frac{d^3k}{(2\pi)^3}\frac{1}{4\omega_\pi\omega_\rho}\left[\frac{(1+n^\pi)L_1^{\mu\nu}+n^\rho L_3^{\mu\nu}}{q_0-\omega_\pi-\omega_\rho+i\eta\epsilon(q_0)}+\frac{-n^\pi L_1^{\mu\nu}+n^\rho L_4^{\mu\nu}}{q_0-\omega_\pi+\omega_\rho+i\eta\epsilon(q_0)}\right. \\ & \left.+\frac{n^\pi L_2^{\mu\nu}-n^\rho L_3^{\mu\nu}}{q_0+\omega_\pi-\omega_\rho+i\eta\epsilon(q_0)}+\frac{-n^\pi L_2^{\mu\nu}-(1+n^\rho)L_4^{\mu\nu}}{q_0+\omega_\pi+\omega_\rho+i\eta\epsilon(q_0)}\right]\end{aligned} \tag{20}$$

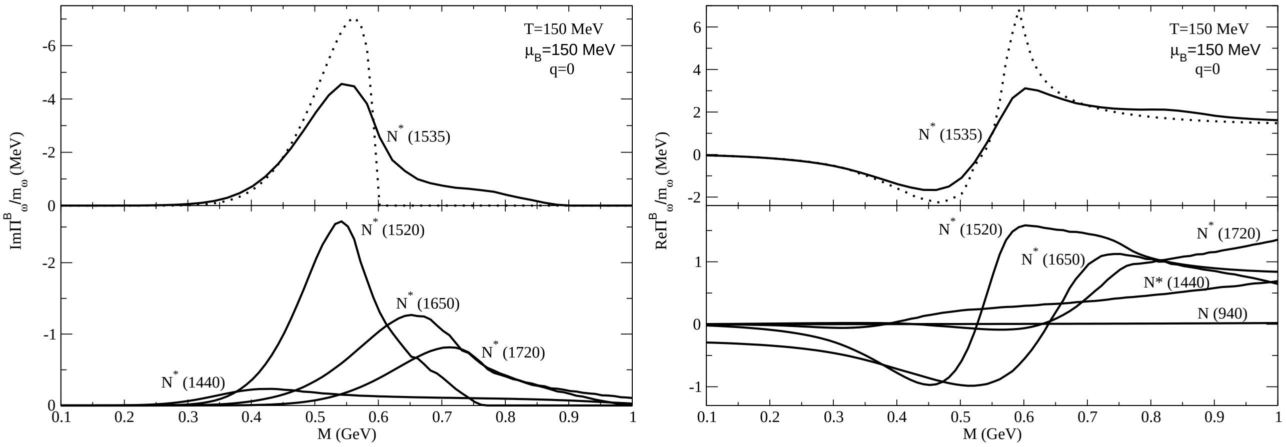

Figure 2: Left: The upper panel shows the contribution of the $NN^*(1535)$ loop where the result in the narrow width approximation is indicated by the dotted line. The lower panel shows the contribution of other NB loops. Right: The corresponding results for the real part.

where $n^\pi = n(\omega_\pi)$ with $\omega_\pi = \sqrt{\vec{k}^2 + m_\pi^2}$ and $n^\rho = n(\omega_\rho)$ with $\omega_\rho = \sqrt{(\vec{q}-\vec{k})^2 + m_\rho^2}$. Here, unlike the baryon loops both the Landau and unitary cuts are relevant for the imaginary part in the kinematic domain of our interest. These are respectively given by

$$\mathrm{Im}\overline{\Pi}^{\mu\nu}_{(\rho\pi)} = -\frac{\epsilon(q_0)}{16\pi|\vec{q}|}\int_{\widetilde{\omega}_\pi^+}^{\widetilde{\omega}_\pi^-} d\widetilde{\omega}_\pi L_2^{\mu\nu}\{n(\widetilde{\omega}_\pi) - n(\widetilde{\omega}_\rho = q_0 + \widetilde{\omega}_\pi)\} \tag{21}$$

and

$$\mathrm{Im}\overline{\Pi}^{\mu\nu}_{(\rho\pi)} = -\frac{\epsilon(q_0)}{16\pi|\vec{q}|}\int_{\omega_\pi^-}^{\omega_\pi^+} d\omega L_1^{\mu\nu}\{1 + n(\omega_\pi) + n(q_0 - \omega_\pi)\} \tag{22}$$

where the integration limits $\omega_\pi^\pm = \frac{S_\pi^2}{2q^2}(q_0 \pm |\vec{q}|W_\pi)$, $\widetilde{\omega}_\pi^\pm = \frac{S_\pi^2}{2q^2}(-q_0 \pm |\vec{q}|W_\pi)$ with $W_\pi = \sqrt{1 - \frac{4q^2 m_\pi^2}{S_\pi^4}}$ and $S_\pi^2 = q^2 - m_\rho^2 + m_\pi^2$.

The real part of the self-energy can be easily read off from (20) in terms of principal value integrals and we do not write them here.

The ω self-energy due to its coupling to 3π states can be estimated by folding the $\rho\pi$ contribution with the ρ spectral function A_ρ as in [8] getting

$$\overline{\Pi}^{\mu\nu}_M(q) = \frac{1}{N_\rho}\int_{4m_\pi^2}^{(q-m_\pi)^2} dM^2[\overline{\Pi}^{\mu\nu}_{(\rho\pi)}(q,M)]A_\rho(M) \tag{23}$$

where $N_\rho = \int_{4m_\pi^2}^{(q-m_\pi)^2} dM^2 A_\rho(M)$ and A_ρ is the ρ spectral function.

Following [22, 14], the Landau cut contribution from the $\rho\pi$ loop can be interpreted as the probability of occurrence of processes like $\omega\pi \to \rho$ and $\omega\rho \to \pi$ which are responsible for the loss of ω mesons in the medium minus the reverse processes which lead to a gain. Similarly, the unitary cut contribution accounts for processes like $\omega \to \rho\pi$ and its reverse. As a consequence of folding with the ρ spectral function containing its 2π decay width, all possible scatterings like $\omega\pi \to \pi\pi$, $\omega\pi\pi \to \pi$ etc. as well as the decay $\omega \to 3\pi$, proceeding through ρ-exchange are effectively accounted for in the imaginary part.

4 Results and discussion

We now present the results of numerical evaluation. We start with the spin-averaged self-energy function defined as

$$\overline{\Pi} = \frac{1}{3}(2\overline{\Pi}_t + q^2\overline{\Pi}_l) \tag{24}$$

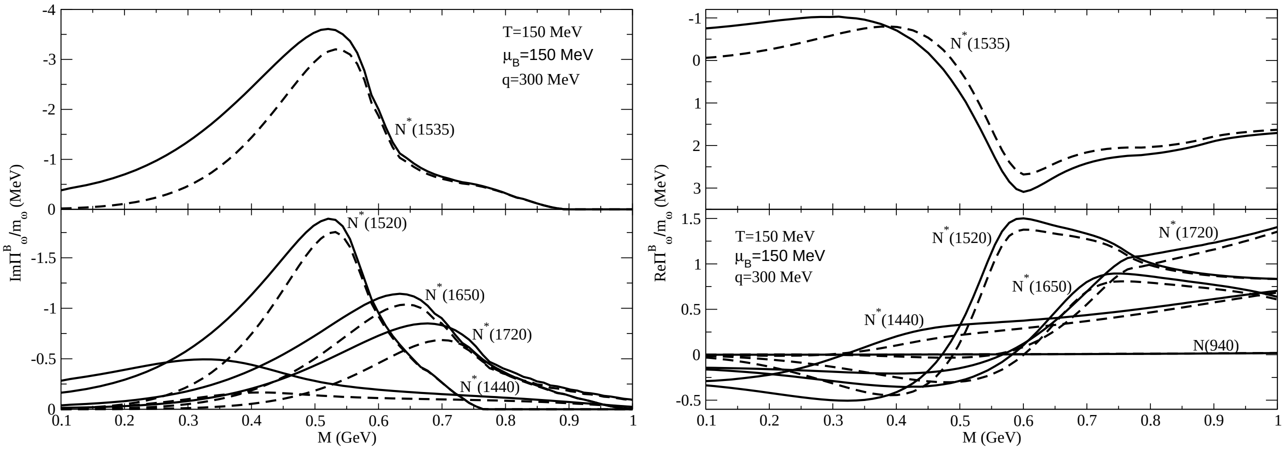

Figure 3: Imaginary (left) and real (right) parts of ω self energy for the NB loops with three-momentum $q = 300$ MeV. Solid and dotted lines stand for transverse and longitudinal part of the self energy respectively.

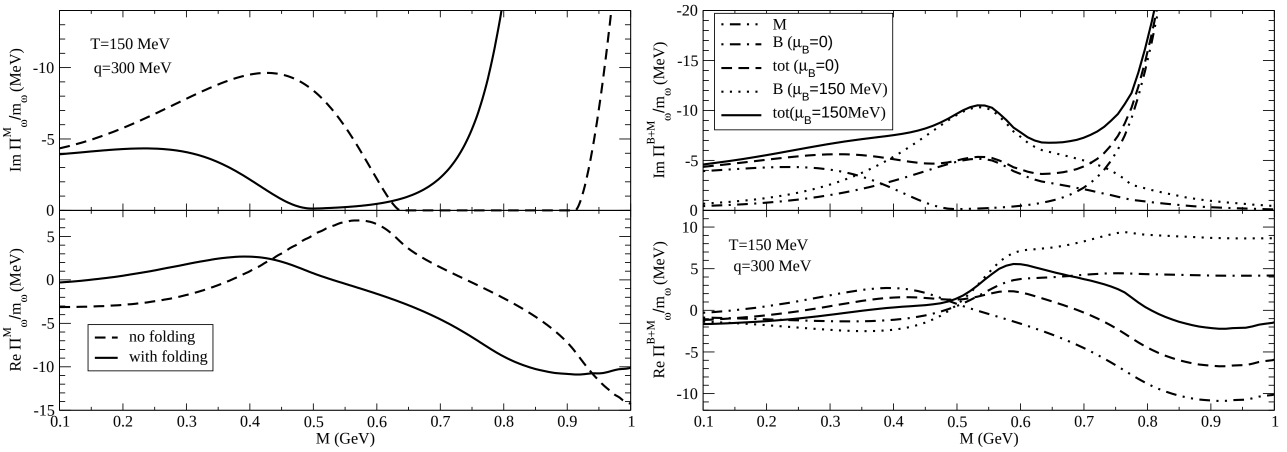

Figure 4: Left panel shows imaginary (upper panel) and real (lower panel) part of ω self energy for mesonic loop with and without the convolution with the ρ spectral function. The right panel shows the total imaginary (upper panel) and real (lower panel) parts of ω self energy for meson and baryon loops.

where $\overline{\Pi}_{t,l}$ are defined in eq. (9). In Fig. 2 we plot the imaginary and real parts of ω self-energy for vanishing three-momentum in the left and right panels respectively. The contribution of the $NN^*(1535)$ loop is observed to play the most significant role primarily due to the strong coupling of this resonance with the ωN channel and is shown separately in the upper panels. The effect of folding by the spectral function of the resonances denoted by B is also shown where the smoothing of the sharp cut-off in the imaginary part defining the end of the Landau cut is clearly observed in the upper panel on the left. In the lower panels showing the contribution of the other loops the effect of the $N*(1520)$ is seen to be significantly more than the others. In the left and right panels of Fig. 3 we have shown the imaginary and real parts of ω self-energy for $\vec{q} = 300$ MeV. Here the transverse component $\overline{\Pi}_t$ is shown along with q^2 times the longitudinal component (note that $\overline{\Pi}_t = q^2\overline{\Pi}_l$ for $\vec{q} = 0$). As before, the $N^*(1535)$ makes the most important contribution and is shown separately in the top panels.

Plotted in the left panel of Fig. 4 is the spin averaged ω self-energy from the $\rho\pi$ loop. The effect of folding the $\rho\pi$ self-energy with the ρ width is clearly visible in the upper panel by the solid line which shows a finite contribution at the ω pole instead of a vanishing contribution in this region when this folding is not done, as shown by the dashed line. This is because the ω pole lies in between the Landau and unitary cut thresholds at ∼630 and ∼910 MeV respectively. On the right panel is shown the total contribution from the meson and baryon loops for two values of the baryon chemical potential. A noticeable contribution is seen in the imaginary part below the nominal ω mass. In the lower panel is shown the real part where the

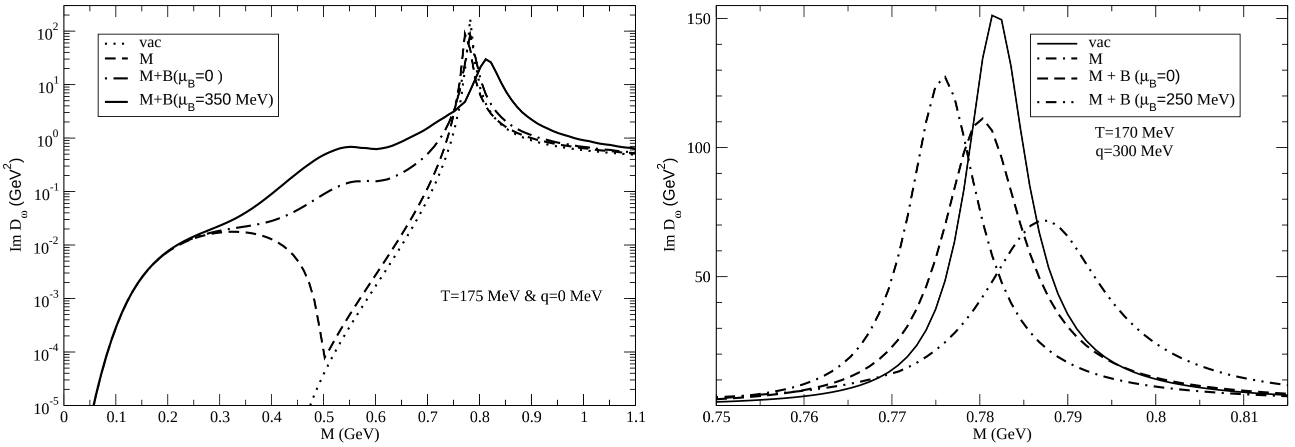

Figure 5: Left: The ω spectral function showing individual contributions due to mesonic and baryonic loops. Right: The region close to the ω pole.

meson and baryon loops provide a negative and positive contribution respectively at the ω pole which will be manifested in the spectral function.

We now turn to the results for the spin averaged spectral function of the ω which is defined as

$$\mathrm{Im}\,\overline{D}(q) = \frac{1}{3}(2\mathrm{Im}\,\overline{D}_t + q^2\mathrm{Im}\,\overline{D}_l) \tag{25}$$

where the transverse and longitudinal components are associated with the corresponding projectors $P_{\mu\nu}$ and $Q_{\mu\nu}$ respectively. These are given by

$$\mathrm{Im}\,\overline{D}_{t,l}(q) = \frac{-\sum \mathrm{Im}\,\overline{\Pi}^{B+M}_{t,l}}{(q^2 - m_\omega^2 - (1,q^2)\sum \mathrm{Re}\,\overline{\Pi}^{B+M}_{t,l})^2 + \{(1,q^2)\sum \mathrm{Im}\,\overline{\Pi}^{B+M}_{t,l}\}^2}\ . \tag{26}$$

It is interesting to note that the rate of lepton pair production in the late (hadronic) stages of heavy ion collisions is essentially determined by the spectral function of low mass vector mesons, ρ, ω and ϕ. This is given by [23],

$$\frac{dN}{d^4q d^4x} = -\frac{\alpha^2}{3\pi^3 q^2} f_{BE}(q_0) g^{\mu\nu} \sum_{V=\rho,\omega,\phi} \frac{F_V^2}{m_V^2}\ \mathrm{Im}\overline{D}^V_{\mu\nu}(q_0,\vec{q}) \tag{27}$$

where the exact propagator $\overline{D}_{\mu\nu}(q_0,\vec{q})$ for a vector meson V is defined in eq. (6). Using the relations $g^{\mu\nu}P_{\mu\nu} = -2$ and $g^{\mu\nu}Q_{\mu\nu} = -q^2$ we get $\mathrm{Im}\overline{D} = -\frac{1}{3}g^{\mu\nu}\mathrm{Im}\overline{D}_{\mu\nu}$ which is the spin averaged spectral function given by eq. (25). We then have,

$$\frac{dN}{d^4q d^4x} = \frac{\alpha^2}{\pi^3 q^2} f_{BE}(q_0) \sum_{V=\rho,\omega,\phi} \frac{F_V^2}{m_V^2}\ \mathrm{Im}\overline{D}^V(q_0,\vec{q})\ . \tag{28}$$

In Fig. 5 we show the contributions of the different loops to the spectral function. To bring out the relative strengths at low invariant masses a logarithmic scale is employed in the left panel. The dashed line represents $\rho\pi$ loop in which the Landau cut contribution falls off in the vinicity of $M = m_\rho - m_\pi$ and then increases as the unitary cut contribution builds up. The Landau cut contributions from the baryonic loops, shown by the solid and dash-dotted lines, however dominate in the region below the ω mass. We now concentrate on a small M range around the ω mass in the right panel of Fig. 5. In tune with the real part of the self-energy shown in the lower right panel of Fig. 4, the peak shifts a little to the left for the meson loop in contrast to the situation when baryonic contributions are added. The slight increase in mass in this case is also accompanied by a larger imaginary part causing more suppression of the spectral

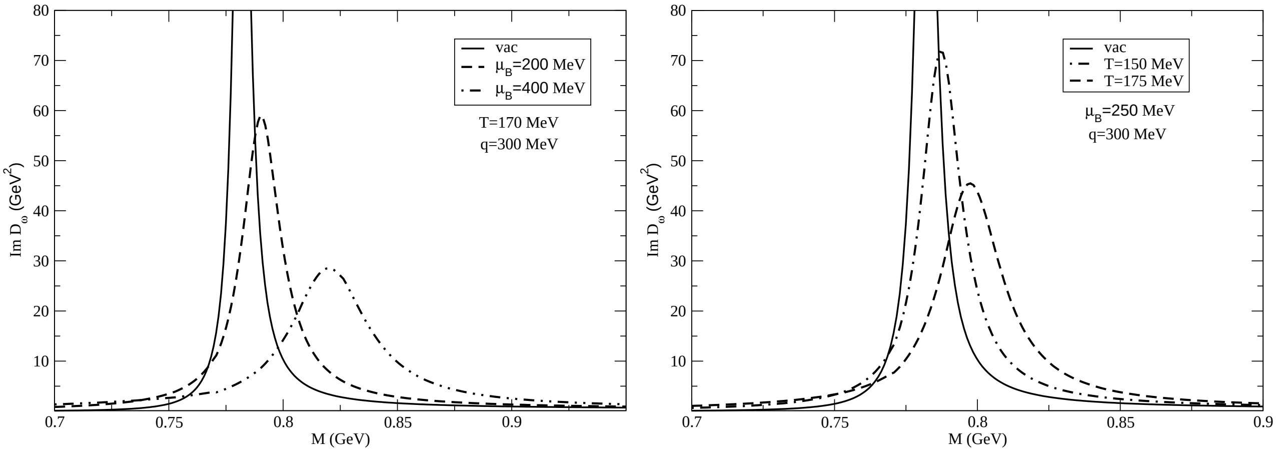

Figure 6: The spectral function of ω for different values of μ_B (left) and T (right)

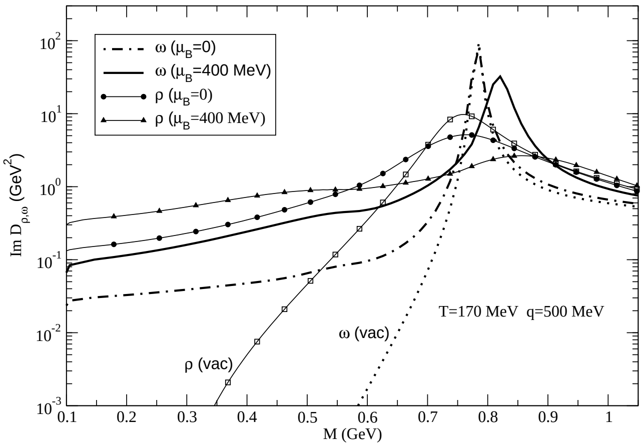

Figure 7: The ω spectral function seen in comparison with the ρ.

strength at the peak. Next we plot the spectral function for different μ_B and T in the left and right panels of Fig. 4 respectively for M close to the ω mass. As before, the small positive thermal mass shift of the ω increases with μ_B and T. The corresponding decrease of the ω-spectral function at the peak representing the enhancement of width with increasing μ_B and T is also seen.

In view of the fact that the ρ and ω peaks are close to each other it is worthwhile to compare their relative spectral strengths below their nominal masses. We have plotted the ω spectral function at two values of the chemical potential along with that of the ρ which has been recently calculated in Ref. [15]. The sharp peak of the ω is stands out against the smooth profile of the ρ. The characteristic 2π and 3π thresholds for the ρ and ω in the vacuum case are also visible. Though the spectral strength of the ω is lower than the ρ they do have a sizeable contribution in the region below ~700 MeV.

5 Summary and Discussion

To summarize, we have evaluated the spectral function of the ω meson in hot and dense matter using the framework of thermal field theory in the real-time formulation. Using effective interactions, one-loop self-energy graphs were evaluated for an extensive set of spin one-half and three-half N^* resonances in addition to the $\rho\pi$ loop using fully relativistic propagators and off-shell corrections for spin three-half fields. The imaginary part has been obtained from the discontinuities of the self-energy function which provides an unified treatment of various scattering and decay processes occurring in the thermal medium. Results of the real and imaginary parts for all the loops and the full spectral function were presented for several combinations of temperature and baryon chemical potential relevant in heavy ion collisions.

In view of the significant difference in various approaches to obtain the ω spectral function discussed in the literature, a quantitative comparison with other results does not appear meaningful. We have however made a comparison with the ρ spectral function finding the ω contribution to be lower but of comparable magnitude. However, the fact that the latter is suppressed by a factor ~ 10 compared to the ρ in the dilepton emission rate makes a quantitative study of the ω difficult. Additional hindrances could arise due to matter induced $\rho-\omega$ mixing [24]. Nevertheless, the contribution of the ω spectral strength is essential for a quantitative description of the dilepton data from heavy ion collisions [25]. In view of high quality data expected in future from heavy ion collisions at the FAIR facility at GSI we can conclude that a detailed evaluation of the spectral strength at finite temperature and baryon density is necessary for a quantitative analysis.

6 Appendix

6.1 Interaction Lagrangian and expressions for $L_{\mu\nu}$ for baryonic loops

The ωN couplings with the resonances are described by the interaction Lagrangians [8]

$$\begin{aligned}
\mathcal{L} &= -[\overline{\psi}_B(g_1\gamma_\mu - \frac{g_2}{2m_N}\sigma_{\mu\nu}\partial^\nu_\omega)\psi_N\omega^\mu + h.c.] && J^P_B = \frac{1}{2}^+ \\
\mathcal{L} &= i[\overline{\psi}_B\gamma^5(g_1\gamma_\mu - \frac{g_2}{2m_N}\sigma_{\mu\nu}\partial^\nu_\omega)\psi_N\omega^\mu + h.c.] && J^P_B = \frac{1}{2}^- \\
\mathcal{L} &= -i[\overline{\psi}^\mu_B\gamma^5(\frac{g_1}{2m_N}\gamma^\alpha + i\frac{g_2}{4m_N^2}\partial^\alpha_N + i\frac{g_3}{4m_N^2}\partial^\alpha_\omega)(\partial^\omega_\alpha\mathcal{O}_{\mu\nu} - \partial^\omega_\mu\mathcal{O}_{\alpha\nu})\psi_N\omega^\nu + h.c.] && J^P_B = \frac{3}{2}^+ \\
\mathcal{L} &= -[\overline{\psi}^\mu_B(\frac{g_1}{2m_N}\gamma^\alpha + i\frac{g_2}{4m_N^2}\partial^\alpha_N + i\frac{g_3}{4m_N^2}\partial^\alpha_\omega)(\partial^\omega_\alpha\mathcal{O}_{\mu\nu} - \partial^\omega_\mu\mathcal{O}_{\alpha\nu})\psi_N\omega^\nu + h.c.] && J^P_B = \frac{3}{2}^- \qquad \text{(A.1)}
\end{aligned}$$

where $\sigma^{\mu\nu} = \frac{i}{2}[\gamma^\mu\gamma^\nu - \gamma^\nu\gamma^\mu]$ and $\mathcal{O}_{\mu\nu} = g_{\mu\nu} - \frac{1}{4}\gamma_\mu\gamma_\nu$ is the off-shell projector contracted with the vertices containing spin 3/2 fields [26] which contributes only when it is off the mass shell. The values of all the coupling constants in the ωNB Lagrangian are taken from Ref. ([8, 27]) and are given below in Table 1.

For spin $\frac{1}{2}^\pm$ resonances the tensor $L^{\mu\nu}(k,q)$ of eq. (14) is given by

$$L^{\mu\nu}(k,q) = -tr[(g_1\gamma^\mu + i\frac{g_2}{2m_N}\sigma^{\mu\alpha}q_\alpha)(\not{k} + bm_N)(g_1\gamma^\mu - i\frac{g_2}{2m_N}\sigma^{\mu\alpha}q_\alpha)(\not{k} + a\not{q} + m_B)] \qquad \text{(A.2)}$$

where $b = \pm 1$ for $J^P = \frac{1}{2}^\pm$ resonances.

Considering only the four-dimensionally transverse part of the self-energy we have

$$L^{\mu\nu} = 4(\frac{g_2}{2m_N})^2[(k^2 - a(q\cdot k) + bm_Nm_B)q^2A^{\mu\nu} + 2B^{\mu\nu} + (0)C^{\mu\nu}] \qquad \text{(A.3)}$$

with

$$\begin{aligned}
A_{\alpha\beta}(q) &= -g_{\alpha\beta} + q_\alpha q_\beta/q^2, \\
B_{\alpha\beta}(k,q) &= q^2k_\alpha k_\beta - q\cdot k(q_\alpha k_\beta + k_\alpha q_\beta) + (q\cdot k)^2g_{\alpha\beta}, \\
C_{\alpha\beta}(k,q) &= q^4k_\alpha k_\beta - q^2(q\cdot k)(q_\alpha k_\beta + k_\alpha q_\beta + (q\cdot k)^2q_\alpha q_\beta. \qquad \text{(A.4)}
\end{aligned}$$

For spin $\frac{3}{2}^\pm$ resonances

$$L^{\mu\nu}(k,q) = -tr[V^{\mu\alpha}(\not{k} + bm_N)V^{\nu\beta}(\not{k} + a\not{q} + m_B)K_{\beta\alpha}] \qquad \text{(A.5)}$$

B	J^P	g_1	g_2	g_3
$N(940)$	$\frac{1}{2}^+$	4.19	-0.79	-
$N^*(1440)$	$\frac{1}{2}^+$	1.53	-4.35	-
$N^*(1520)$	$\frac{3}{2}^-$	3.35	4.80	-9.99
$N^*(1535)$	$\frac{1}{2}^-$	3.79	6.50	-
$N^*(1650)$	$\frac{1}{2}^-$	-1.13	-3.27	-
$N^*(1720)$	$\frac{3}{2}^+$	-6.82	-5.84	-8.63

Table 1: Table showing the coupling constants of ωNB vertex where B stands for various resonances considered.

where $V^{\mu\alpha} = V_0^{\mu\alpha} + cV_c^{\mu\alpha}$ for the off shell projection operator $\mathcal{O}_{\mu\nu} = g_{\mu\nu} + c\gamma_\mu\gamma_\nu$ (i.e. $c = -\frac{1}{4}$) with

$$\begin{aligned} V_0^{\mu\alpha} &= \frac{g_1}{2m_N}(\not{q}g^{\mu\alpha} - \gamma^\mu q^\alpha) + \frac{g_2}{4m_N^2}\{(q\cdot k)g^{\mu\alpha} - k^\mu q^\alpha\} - \frac{g_3}{4m_N^2}(q^2 g^{\mu\alpha} - q^\mu q^\alpha) \\ V_c^{\mu\alpha} &= \frac{g_1}{2m_N}\gamma^\mu(\gamma^\alpha\not{q} - \not{q}\gamma^\alpha) + \frac{g_2}{4m_N^2}\gamma^\mu\{\gamma^\alpha(q\cdot k) - \not{q}k^\alpha\} - \frac{g_3}{4m_N^2}\gamma^\mu(q^2\gamma^\alpha - \not{q}q^\alpha)\ . \end{aligned} \tag{A.6}$$

Here b indicates the parity states of spin 3/2 resonances i.e. $b = \pm 1$ for $J^P = \frac{3}{2}^\pm$. Considering all three coupling constants $L^{\mu\nu}$ is given by

$$L^{\mu\nu} = (\frac{g_1}{2m_N})^2 L_{11}^{\mu\nu} + (\frac{g_2}{4m_N^2})^2 L_{22}^{\mu\nu} + (\frac{g_3}{4m_N^2})^2 L_{33}^{\mu\nu} + \frac{g_1}{2m_N}\frac{g_2}{4m_N^2}L_{12}^{\mu\nu} + \frac{g_1}{2m_N}\frac{g_3}{4m_N^2}L_{13}^{\mu\nu} + \frac{g_2}{4m_N^2}\frac{g_3}{4m_N^2}L_{23}^{\mu\nu} \tag{A.7}$$

where

$$L_{ij}^{\mu\nu} = (\alpha_{ij}^{00} + c\alpha_{ij}^{0c} + c^2\alpha_{ij}^{cc})A^{\mu\nu} + (\beta_{ij}^{00} + c\beta_{ij}^{0c} + c^2\beta_{ij}^{cc})B^{\mu\nu} + (\gamma_{ij}^{00} + c\gamma_{ij}^{0c} + c^2\gamma_{ij}^{cc})C^{\mu\nu} \tag{A.8}$$

with six possible sets of ij ($ij = 11, 22, 33, 12, 13$ and 23). The values of the coefficients for each set are given by

$$\begin{aligned}
\alpha_{11}^{00} &= \frac{8}{3m_B^2}[(k^2m_B^2 + bm_Nm_B^3 - k^2q^2) - a(q\cdot k)(2k^2 + q^2 + 2a(q\cdot k))]q^2 \\
\beta_{11}^{00} &= \frac{8}{3m_B^2}[k^2 + m_B^2 + a(q\cdot k)] \\
\alpha_{11}^{0c} &= 4\frac{8}{3m_B^2}[bm_Nm_BS_N^2 - a(q\cdot k)(S_N^2 + 3a(q\cdot k) - 2bm_Nm_B)]q^2 \\
\beta_{11}^{0c} &= 4\frac{8}{3m_B^2}[k^2 - m_B^2 + 2a(q\cdot k)] \\
\gamma_{11}^{0c} &= 4\frac{8}{3m_B^2} \\
\alpha_{11}^{cc} &= 4\frac{8}{3m_B^2}[(m_N^2 + 2bm_Nm_B)\{S_N^2 + 2a(q\cdot k)\} - a(q\cdot k)\{S_N^2 + 4a(q\cdot k)\}]q^2 \\
\beta_{11}^{cc} &= 4\frac{8}{3m_B^2}[2\{k^2 - m_B^2 + 2a(q\cdot k)\}] \\
\gamma_{11}^{cc} &= 4\frac{8}{3m_B^2}[2]
\end{aligned} \tag{A.9}$$

$$\begin{aligned}
\beta_{22}^{00} &= \frac{8}{3m_B^2}[\{k^2 - bm_Nm_B + a(q\cdot k)\}m_B^2] \\
\gamma_{22}^{00} &= \frac{8}{3m_B^2}[-k^2 + bm_Nm_B - a(q\cdot k)] \\
\beta_{22}^{0c} &= \frac{8}{3m_B^2}[-bm_Nm_B\{S_N^2 + 2a(q\cdot k)\}] \\
\beta_{22}^{cc} &= \frac{8}{3m_B^2}[a(q\cdot k)\{S_N^2 + 2a(q\cdot k)\}] \\
\gamma_{22}^{cc} &= \frac{8}{3m_B^2}[(k^2 - bm_Nm_B)\{S_N^2 + 2a(q\cdot k)\}]
\end{aligned} \tag{A.10}$$

$$\begin{aligned}
\alpha_{33}^{00} &= \frac{8}{3m_B^2}[\{-k^2 + bm_Nm_B - a(q\cdot k)\}m_B^2]q^4 \\
\gamma_{33}^{00} &= \frac{8}{3m_B^2}[-k^2 + bm_Nm_B - a(q\cdot k)] \\
\alpha_{33}^{0c} &= \frac{8}{3m_B^2}[bm_Nm_B\{S_N^2 + 2a(q\cdot k)\}]q^4 \\
\gamma_{33}^{0c} &= \frac{8}{3m_B^2}[-2\{S_N^2 + 2a(q\cdot k)\}] \\
\alpha_{33}^{cc} &= \frac{8}{3m_B^2}[\{k^2 - 2bm_Nm_B + a(q\cdot k)\}\{S_N^2 + 2a(q\cdot k)\}]q^4 \\
\gamma_{33}^{cc} &= \frac{8}{3m_B^2}[-2\{S_N^2 + 2a(q\cdot k)\}]
\end{aligned} \tag{A.11}$$

$$\begin{aligned}
\alpha_{12}^{00} &= \frac{8}{3m_B^2}[-k^2 + 2bm_N m_B - a(q\cdot k)]m_B(q\cdot k)q^2 \\
\beta_{12}^{00} &= \frac{8}{3m_B^2}[k^2 - 2bm_N m_B + a(q\cdot k) + m_B^2]m_B \\
\gamma_{12}^{00} &= \frac{8}{3m_B^2}[-m_B] \\
\alpha_{12}^{0c} &= 2\frac{8}{3m_B^2}[abm_N(q\cdot k)\{S_N^2 + 2a(q\cdot k)\}]q^2 \\
\beta_{12}^{0c} &= 2\frac{8}{3m_B^2}[(2m_B - bm_N)\{S_N^2 + 2a(q\cdot k)\}] \\
\alpha_{12}^{cc} &= 4\frac{8}{3m_B^2}[abm_N(q\cdot k)\{S_N^2 + 2a(q\cdot k)\}]q^2 \\
\beta_{12}^{cc} &= 4\frac{8}{3m_B^2}[(2m_B - bm_N)\{S_N^2 + 2a(q\cdot k)\}]
\end{aligned} \tag{A.12}$$

$$\begin{aligned}
\alpha_{13}^{00} &= \frac{8}{3m_B^2}[(k^2 + q^2 + m_B^2 - 2bm_N m_B)(q\cdot k) + aq^2(k^2 - 2bm_N m_B)]m_B q^2 \\
\beta_{13}^{00} &= \frac{8}{3m_B^2}[-am_B q^2] \\
\alpha_{13}^{0c} &= 2\frac{8}{3m_B^2}[\{(2m_B - bm_N)(q\cdot k) - abm_N q^2\}\{S_N^2 + 2a(q\cdot k)\}]q^2 \\
\alpha_{13}^{cc} &= 4\frac{8}{3m_B^2}[\{(2m_B - bm_N)(q\cdot k) - abm_N q^2\}\{S_N^2 + 2a(q\cdot k)\}]q^2
\end{aligned} \tag{A.13}$$

$$\begin{aligned}
\alpha_{23}^{00} &= 2\frac{8}{3m_B^2}[k^2 - 2bm_N m_B + a(q\cdot k)]m_B^2(q\cdot k)q^2 \\
\gamma_{23}^{00} &= 2\frac{8}{3m_B^2}[-a\{k^2 - 2bm_N m_B + a(q\cdot k)\}] \\
\alpha_{23}^{0c} &= 2\frac{8}{3m_B^2}[-bm_N m_B(q\cdot k)\{S_N^2 + 2a(q\cdot k)\}]q^2 \\
\gamma_{23}^{0c} &= 2\frac{8}{3m_B^2}[-a\{S_N^2 + 2a(q\cdot k)\}] \\
\alpha_{23}^{cc} &= 2\frac{8}{3m_B^2}[(k^2 - 2bm_N m_B)(q\cdot k)\{S_N^2 + 2a(q\cdot k)\}]q^2 \\
\beta_{23}^{cc} &= 2\frac{8}{3m_B^2}[-a\{S_N^2 + 2a(q\cdot k)\}]q^2
\end{aligned} \tag{A.14}$$

The rest of the coefficients are zero.

6.2 Interaction Lagrangian and expressions for $L_{\mu\nu}$ for mesonic loops

For the interaction vertices entering the self-energy graphs for mesonic loops, we expand the relevant terms of the chiral Lagrangian and retain the lowest order terms to get [28, 29]

$$\mathcal{L}_{int} = \frac{g_m}{F_\pi}\epsilon_{\mu\nu\lambda\sigma}(\partial^\nu\omega^\mu\vec{\rho}^\lambda - \omega^\mu\partial^\nu\vec{\rho}^\lambda)\cdot\partial^\sigma\vec{\pi}\ . \tag{A.15}$$

Here, the pion decay constant, $F_\pi = 93$ MeV. The decay rate $\Gamma(\omega \to 3\pi) = 7.6$ MeV gives $g_m = 5.5$.

The expression for $L^{\mu\nu}$ appearing in the ω self-energy for the $\pi\rho$ loop is given by,

$$L^{\mu\nu}_{(\rho\pi)}(q,k) = -4\left(\frac{g_m}{F_\pi}\right)^2 (B_{\mu\nu} + q^2k^2A_{\mu\nu}) \tag{A.16}$$

References

[1] J. Alam, S. Sarkar, P. Roy, T. Hatsuda and B. Sinha, Annals Phys. **286**, 159 (2001)

[2] B. Friman, C. Hohne, J. Knoll, S. Leupold, J. Randrup, R. Rapp and P. Senger, in *The CBM physics book: Compressed baryonic matter in laboratory*, Lect. Notes Phys. **814**, 1 (2011).

[3] S. Sarkar, Nucl. Phys. A **862-863**, 13 (2011).

[4] R. S. Hayano and T. Hatsuda, Rev. Mod. Phys. **82** (2010) 2949.

[5] S. Leupold, V. Metag and U. Mosel, Int. J. Mod. Phys. **E 19**, 147 (2010)

[6] F. Klingl, N. Kaiser and W. Weise Nucl. Phys. **A 624**, 527 (1997)

[7] M. F. M. Lutz, G. Wolf and B. Friman, Nucl. Phys. A **706** (2002) 431 [Erratum-ibid. A **765** (2006) 431]

[8] P. Muehlich, V. Shklyar, S. Leupold, U. Mosel, M. Post, Nucl. Phys. A **780**, 187 (2006).

[9] E325 Collaboration, K. Ozawa *et al.*, Phys. Rev. Lett. **86** (2001) 5019

[10] CBELSA/TAPS Collaboration, D. Trnka *et al.*, Phys. Rev. Lett. **94**, 192303 (2005).

[11] R. A. Schneider, W. Weise, Phys. Lett. **B 515**, 89 (2001).

[12] V. L. Eletsky, M. Belkacem, P. J. Ellis and J. I. Kapusta, Phys. Rev. C **64**, 035202 (2001)

[13] R. Rapp, Phys. Rev. C **63**, 054907 (2001)

[14] S. Ghosh, S. Sarkar and S. Mallik, Eur. Phys. J. C **70**, 251 (2010).

[15] S. Ghosh and S. Sarkar, Nucl. Phys. **A 870-871**, 94 (2011).

[16] S. Ghosh, S. Sarkar and S. Mallik, Phys. Rev. **C 83**, 018201 (2011).

[17] M. Le Bellac, *Thermal Field Theory* (Cambridge University Press, Cambridge, 1996).

[18] S. Mallik and S. Sarkar, Eur. Phys. J. C **61**, 489 (2009).

[19] R.L. Kobes and G.W. Semenoff, Nucl. Phys. **B260**, 714 (1985).

[20] B. D. Serot and J. D. Walecka, Adv. Nucl. Phys. **16**, 1 (1986).

[21] S. Sarkar, E. Oset and M. J. Vicente Vacas, Nucl. Phys. A **750**, 294 (2005).

[22] H. A. Weldon, Phys. Rev. D **28** (1983) 2007.

[23] S. Ghosh, S. Sarkar and J. Alam, Eur. Phys. J. C **71** (2011) 1760

[24] P. Roy, A.K. Dutt-Mazumder, S. Sarkar, J. Alam, J. Phys. **G 35**, 065106 (2008)

[25] S. Sarkar and S. Ghosh, arXiv:1204.0893 [nucl-th].

[26] R. D. Peccei, Phys. Rev. **176**, 1812 (1968).

[27] V. Shklyar, H. Lenske, U. Mosel, and G. Penner Phys. Rev. C **71**, 055206 (2005).

[28] G. Ecker, J. Gasser, H. Leutwyler, A. Pich, E. de Rafael, Phys. Lett. B 223 425 (1989).

[29] S. Mallik, S. Sarkar, Eur. Phys. J. C 25, 445 (2002)